NASA TECHNICAL NOTE

NASA TN D-3598

ANALYSIS OF HEAT-REJECTION CHARACTERISTICS OF SPACE RADIATOR PANELS UTILIZING SHARED FINS

by Mario A. Colaluca, Henry C. Haller, and Seymour Lieblein

Lewis Research Center
Cleveland, Ohio

NATIONAL AERONAUTICS AND SPACE ADMINISTRATION • WASHINGTON, D. C. • AUGUST 1966

NASA TN D-3598

ANALYSIS OF HEAT-REJECTION CHARACTERISTICS OF SPACE RADIATOR PANELS UTILIZING SHARED FINS

By Mario A. Colaluca, Henry C. Haller, and Seymour Lieblein

Lewis Research Center
Cleveland, Ohio

NATIONAL AERONAUTICS AND SPACE ADMINISTRATION

For sale by the Clearinghouse for Federal Scientific and Technical Information
Springfield, Virginia 22151 – Price $2.00

ANALYSIS OF HEAT-REJECTION CHARACTERISTICS OF SPACE RADIATOR PANELS UTILIZING SHARED FINS

by Mario A. Colaluca, Henry C. Haller, and Seymour Lieblein

Lewis Research Center

SUMMARY

An analytical study was performed to provide information on the heat radiated to space from three radiator finned-tube configurations used in a shared-fin radiator. A shared-fin radiator panel contains multiple independent heat-transfer circuits, so that adjacent tubes sharing the fin between them are fed by different circuits. Numerical results for the heat-transfer characteristics of these configurations for the case of loss of heat-transfer fluid in one tube circuit were obtained under the condition that all radiating surfaces act as blackbodies. For the case of two independent tube circuits with one circuit inoperative, the heat-rejection rate for the three geometries ranged from 55 to 65 percent of the value with all circuits functioning properly.

For the case of one tube circuit inoperative, the shared-fin arrangement (multiple independent tube circuits) offered an advantage in heat-rejection capability over the simply segmented arrangement (multiple independent panels) that decreased with the design number of circuits. For two independent circuits, the shared-fin heat rejection after puncture was from 10 to 30 percent greater than for the simply segmented radiator over the range of conditions investigated. For four circuits, the shared fin's advantage was reduced to 3 to 9 percent.

INTRODUCTION

The use of radiating fins to augment the heat-transfer capabilities of waste-heat radiators for space power generating systems has been shown to be a feasible concept. Numerous analytical studies have been carried out to determine the heat-rejection performance of fins that depend on heat conduction to transfer the heat from a fluid-carrying tube to the surfaces of the fin. Typical fin-tube geometries that are under consideration

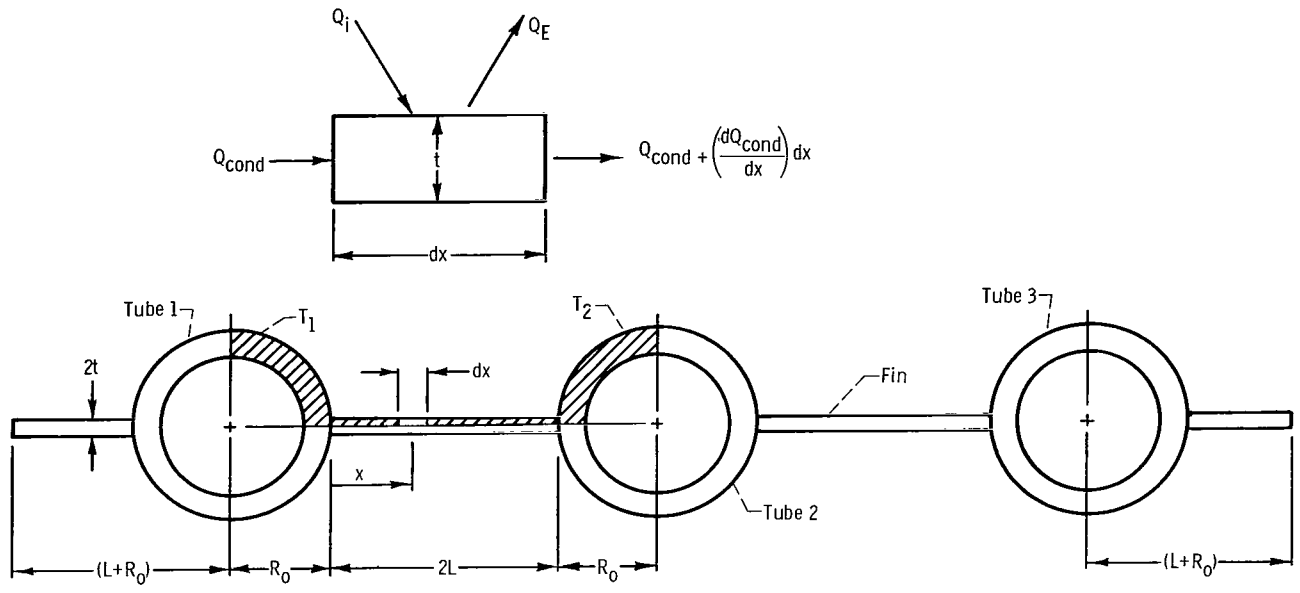

(a) Central fin tube; $\ell = L$.

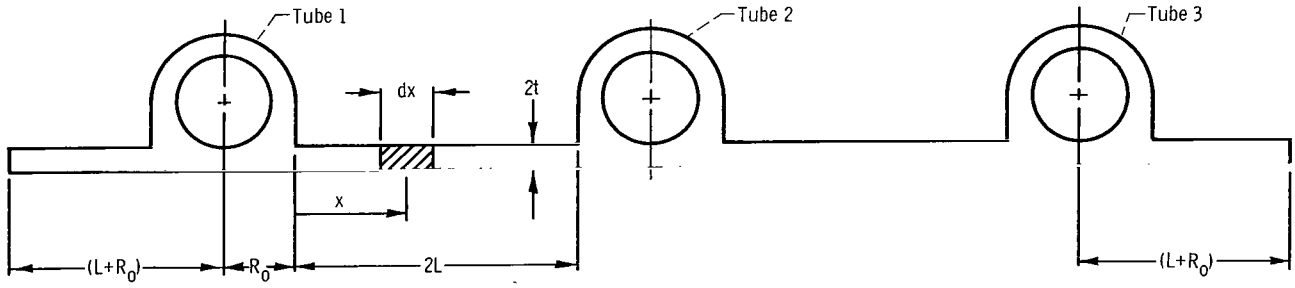

(b) Open fin tube; $\ell = L$.

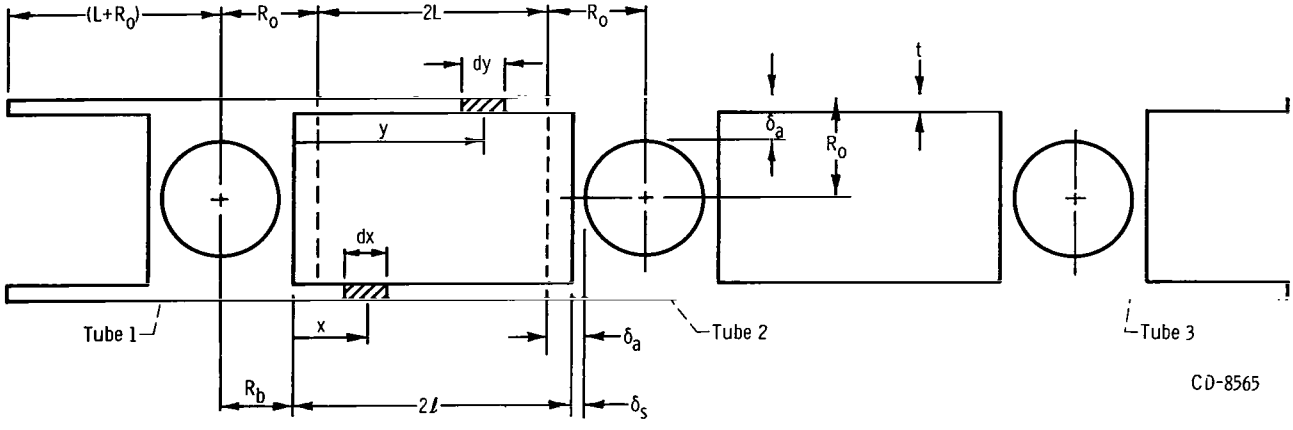

(c) Double fin tube; $\ell = L+\delta_a (1-\delta_s/\delta_a)$.

Figure 1. - Fin-tube geometries studied.

for use in conventional space radiators are the solid-conducting central, double, and open fin-tube configurations (fig. 1), which are described in detail in references 1 to 5.

A critical problem faced in the design of heat-rejection systems is that of vulnerability of the system to catestrophic meteoroid puncture. One solution to this problem is to provide parallel circuits in the radiator system so that the puncture of a tube would not result in a total loss of working fluid. A simple way to provide parallel circuits would be to use several isolatable panels, each with its independent fluid circuit (fig. 2(a)). This concept is referred to as a simply segmented radiator system (refs. 6 and 7). In such an arrangement, a tube puncture would result in the loss of only the panel segment containing the punctured tube. Another approach to the problem is the use of the shared-fin concept. A single-panel shared-fin radiator contains multiple independent heat-transfer circuits so that adjacent tubes sharing the fin between them are fed by different circuits (fig. 2(b)).

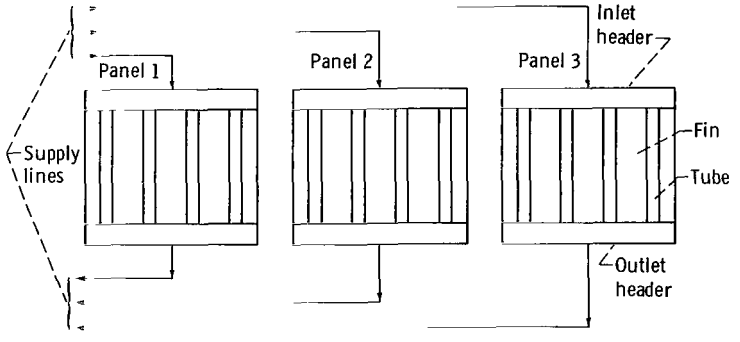

(a) Simply segmented radiator.

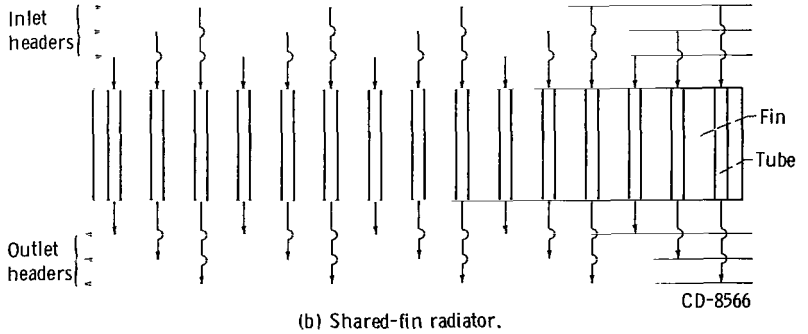

(b) Shared-fin radiator.

Figure 2. - Radiator concepts.

If a tube is punctured, inactivating the fluid circuit containing the tube, the fins associated with the punctured tube can still act as fins of the adjacent operating tubes. Although the temperature level of the punctured tube and fin will be less than that of the adjacent operating tubes (fig. 3), some radiation will continue to occur from the surfaces of the inoperative circuit. Thus the radiating effectiveness of the radiator will not be degraded in

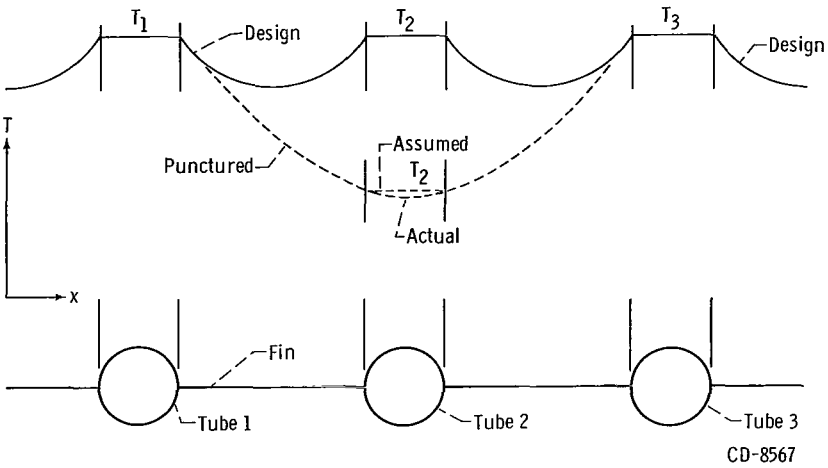

Figure 3. - Typical temperature profiles for design - and punctured-tube cases.

direct proportion to the number of lost circuits, as is the case for the simply segmented panels.

In the application of the shared-fin concept, any number of tube circuits can be utilized for added effectiveness. However, the added complexity and weight of the header arrangement might offset any gain realized through increased radiating effectiveness. A comparative weight analysis of the added circuits, including the weight of the headers, would be necessary to determine the optimum number of circuits. Furthermore, combinations of shared-fin and simply segmented panels can also be used to achieve added flexibility. In any event, evaluation of the usefulness of the shared-fin concept will depend on the magnitude of the radiating effectiveness of the inoperative circuits.

The aim of this investigation is to provide heat-rejection characteristics for three finned-tube geometries used in a shared-fin radiator panel with the fins and tubes in one plane. The analysis has been carried out to provide specific radiating effectiveness data for the case of one circuit punctured for each of the three fin-tube configurations considered, and to compare the overall heat-rejection capabilities of the configurations over a range of design parameters and number of circuits.

ANALYSIS

The three specific finned-tube geometries under consideration in this analysis are shown in figure 1. The development of equations describing the temperature distribution and heat-rejection characteristics for the central fin-tube configuration (fig. 1(a)) will be carried out in detail herein. The analyses for the open fin-tube geometry (fig. 1(b)) and double fin-tube geometry (fig. 1(c)) are presented in an appendix.

Assumptions

The assumptions used in the derivation of the differential equations describing the fin temperature distribution and the punctured tube equilibrium temperature for the central fin-tube configuration as well as for the open and double fin-tube configurations are as follows:

(1) Incident radiation from external sources is negligible.

(2) Radiator surfaces act as blackbodies.

(3) Temperature on the tube outer surface of both functioning and punctured tubes is constant circumferentially and axially.

(4) Steady-state one-dimensional heat flow occurs in the fins with the fin base temperature equal to the temperature of the tube outer surface.

(5) Fin and tube material properties do not vary with temperature.

(6) Development of the fin and tube view factors is based on an infinite axial dimension of fin and tube.

(7) Fin thickness is neglected in the determination of view factors.

Fin Temperature Distribution

Because of the symmetry of the central fin-tube geometry, only the portion of the system shown shaded in figure 1(a) need be considered. A heat balance about an elemental volume (Zt dx) on the fin (fig. 1(a)) yields

$$Q_{cond} + Q_{i,f} = Q_{cond} + \frac{dQ_{cond}}{dx} dx + Q_{E,f} \tag{1}$$

(The symbols are defined in appendix A.) The incident radiant energy $Q_{i,f}$, which arrives from both base surfaces 1 and 2, can be expressed as

$$Q_{i,f} = \sigma T_1^4 F_{1-x} A_1 + \sigma T_2^4 F_{2-x} A_2 \tag{2}$$

where F_{1-x} and F_{2-x} are the view factors (appendix B) from base surfaces 1 and 2 to Z dx. For radiant interchange between surfaces at constant temperature,

$$F_{1-x} A_1 = F_{x-1} Z\, dx$$

and

$$F_{2\text{-}x}A_2 = F_{x\text{-}2}Z\,dx$$

Thus, equation (2) can be expressed as

$$Q_{i,f} = \sigma T_1^4 F_{x\text{-}1} Z\,dx + \sigma T_2^4 F_{x\text{-}2} Z\,dx \tag{3}$$

The energy emitted $Q_{E,f}$ from the elemental volume is given by the Stefan-Boltzman law as

$$Q_{E,f} = \sigma T^4 Z\,dx \tag{4}$$

The conducted heat transferred is given by Fourier's law as

$$Q_{cond} = -kt\,\frac{dT}{dx}Z \tag{5}$$

Substituting equations (3), (4), and (5) into equation (1) and rearranging terms yield

$$kt\,\frac{d^2T}{dx^2} = \sigma T^4 - \sigma\left(T_1^4 F_{x\text{-}1} + T_2^4 F_{x\text{-}2}\right) \tag{6}$$

It is convenient to introduce the nondimensional variables $X = x/2L$, $\theta = T/T_1$, and $\theta_2 = T_2/T_1$ and to define a conductance parameter as

$$N_c = \frac{\sigma T_1^3 \ell^2}{kt} \tag{7}$$

where for the central fin tube $\ell = L$. Introduction of these nondimensional quantities into equation (6) results in

$$\frac{d^2\theta}{dX^2} = 4N_c\left(\theta^4 - F_{X\text{-}1} - F_{X\text{-}2}\theta_2^4\right) \tag{8}$$

Equation (8) along with the boundary conditions

$$\theta = 1 \text{ at } X = 0 \tag{8a}$$

and

$$\theta = \theta_2 \text{ at } X = 1 \tag{8b}$$

describes the one-dimensional temperature distribution in the fin. However, θ_2, the inoperative tube temperature, is as yet unspecified and another equation is needed to complete the solution.

Punctured-Tube Equilibrium Temperature

Prior to the loss of working fluid, the fluid supplies heat to the tube wall, and the tube receives incident radiant energy from adjacent tubes and fin surfaces. Heat is conducted from the tube into the fin, and radiant energy is emitted from the tube outer surface. The heat balance about the tube wall describing this equilibrium situation for the central fin-tube geometry can be written as

$$Q_w + Q_{i,2} = Q_{E,2} + Q_{cond}\Big|_{x=2L} \tag{9}$$

where Q_w is the energy transferred from the working fluid to the tube, and Q_{cond} is the total heat conducted into the fin. The net heat rejected from the radiating surface of the tube can be expressed as

$$Q_R = Q_{E,2} - Q_{i,2} = Q_w - Q_{cond}\Big|_{x=2L} \tag{10}$$

When the working fluid is lost, Q_w goes to zero, and the tube undergoes a transient decrease in internal energy due to the change in net heat transfer. The temperature of the punctured tube will drop until the heat conducted at the fin-tube interface just balances the difference between the heat emitted and that incident at the tube outer surface.

For simplicity, the equilibrium temperature of the punctured tube was assumed to be invariant circumferentially as shown in figure 3 (p. 4). The assumption of invariant circumferential temperature for the punctured tube was verified by a one-dimensional heat-transfer analysis that assumed the punctured tube behaved like a fin with emission off the outer surface. Because the punctured-tube equilibrium temperature is lower than the

design temperature and the incident radiation is greater than the emission, the tube surface temperature will be dictated by the incident energy. Thus, the effects of circumferential conduction in the tube wall are minimized.

The new tube equilibrium condition is described by

$$Q_{E,2} - Q_{i,2} = -Q_{cond}\Big|_{x=2L} \tag{11}$$

The incident energy can be expressed as

$$Q_{i,2} = \sigma T_1^4 F_{1-2} \frac{\pi Z R_o}{2} + \int_0^{2L} \sigma T^4 F_{x-2} Z \, dx \tag{12}$$

The conduction heat transfer is given by

$$-Q_{cond_{x=2L}} = -ktZ \left.\frac{dT}{dx}\right|_{x=2L} \tag{13}$$

where the signs are chosen so that heat conducted into the tube will be positive. The emitted energy by the punctured tube is given by

$$Q_{E,2} = \sigma \frac{\pi R_o}{2} T_2^4 Z \tag{14}$$

where T_2 is the equilibrium temperature of the punctured tube and is different from T_1.

Substituting equations (12), (13), and (14) into equation (11) and introducing the previously mentioned nondimensional variables result in

$$\theta_2^4 = F_{1-2} + \frac{4}{\pi} \frac{L}{R_o} \int_0^1 \theta^4 F_{X-2} \, dX - \frac{\frac{L}{R_o}}{\pi N_c} \left.\frac{d\theta}{dX}\right|_{X=1} \tag{15}$$

The fin temperature distribution and the equilibrium temperature of tube 2 can now be determined by the simultaneous numerical solution of equations (8) and (15) subject to boundary conditions (8a) and (8b).

Radiating Effectiveness

The radiating effectiveness of the punctured central fin-tube three-tube system of figure 1(a) (center tube punctured) (p. 2) can now be determined. Because of symmetry about the centerlines of tubes 1 and 2 and the fin, only the shaded portion of figure 1(a) need be considered.

It is convenient to define the fin-tube radiating effectiveness as the ratio of the heat rejection by the system under consideration to the ideal heat rejection by one side of a fin of width $2(L + R_o)$ at the original base temperature T_1 or

$$\eta_p = \frac{Q_{f,R} + Q_{1,R} + Q_{2,R}}{Q_{id}} \tag{16}$$

where

$$Q_{id} = 2\sigma(L + R_o)T_1^4 Z$$

The remaining quantities in equation (16) (that is, the heat rejected from the upper surface of the fin between the tubes $Q_{f,R}$, from the right quadrant of tube 1, $Q_{1,R}$, and from the left quadrant of tube 2, $Q_{2,R}$) can be obtained from energy balances on the respective surfaces.

For the fin heat rejection, an energy balance about the fin of width $2L$ adjacent to the punctured tube yields the following expression:

$$Q_{cond}\Big|_{x=0} + Q_{i,f} = Q_{E,f} + Q_{cond}\Big|_{x=2L} \tag{17}$$

This can be written as

$$Q_{E,f} - Q_{i,f} = Q_{cond}\Big|_{x=0} - Q_{cond}\Big|_{x=2L} \tag{18}$$

But $Q_{E,f} - Q_{i,f}$ is the net heat radiated by the fin. Thus, by equation (18), the net fin heat rejection can be computed as the difference between the conduction heat transfer at $x = 0$ and that at $x = 2L$. Substituting the proper expressions from Fourier's law for $Q_{cond}\Big|_{x=0}$ and $Q_{cond}\Big|_{x=2L}$ and nondimensionalizing as before, the equation for the net heat rejection from the fin becomes

$$\frac{Q_{f,R}}{\sigma L T_1^4 Z} = -\frac{1}{2N_c}\left[\left(\frac{d\theta}{dX}\right)_{X=0} - \left(\frac{d\theta}{dX}\right)_{X=1}\right] \tag{19}$$

The net heat radiated by the part of tube surface 1 facing the punctured tube is the difference between the emitted and incident energies. The incident energy on a quadrant of the tube surface is the sum of that from the adjacent fin and that from tube 2:

$$Q_{i,1} = \int_0^{2L} ZF_{x-1}\sigma T^4 \, dx + \sigma \frac{\pi}{2} R_o F_{2-1} T_2^4 Z \tag{20}$$

The emitted energy from the tube surface is

$$Q_{E,1} = \sigma \frac{\pi R_o}{2} T_1^4 Z \tag{21}$$

Thus, the net heat radiated by the right quadrant of tube 1 is given by

$$Q_{1,R} = (Q_{E,1} - Q_{i,1})$$

or

$$\frac{Q_{1,R}}{\sigma T_1^4 LZ} = \frac{\pi R_o}{2L} - 2\int_0^1 F_{X-1}\theta^4 \, dX - \frac{\pi R_o}{2L} F_{2-1}\theta_2^4 \tag{22}$$

The net heat radiated by the punctured tube quadrant can be determined from equation (11). The negative heat conducted at the tube-fin interface can be expressed in non-dimensional form as

$$\frac{Q_{2,R}}{\sigma L T_1^4 Z} = -\frac{1}{2N_c}\left.\frac{d\theta}{dX}\right|_{X=1} \tag{23}$$

Substituting equations (19), (22), and (23) into equation (16) yields

$$\eta_p = -\frac{1}{4N_c\left(1+\frac{R_o}{L}\right)}\left(\frac{d\theta}{dX}\right)_{X=0} + \frac{\pi}{4\left(1+\frac{L}{R_o}\right)} - \frac{1}{\left(1+\frac{R_o}{L}\right)}\int_0^1 F_{X-1}\theta^4\, dX - \frac{\pi}{4\left(1+\frac{L}{R_o}\right)}F_{2-1}\theta_2^4 \qquad (24)$$

The fin-tube radiating effectiveness of the three-tube system can be obtained by using equation (24) along with values of $(d\theta/dX)_{X=0}$ and θ^4 obtained from the solution of equation (8) and with θ_2^4 obtained from the solution of equation (15). Equations describing the fin-tube radiating effectiveness of the open and double fin-tube geometries are given in appendix C.

Panel Total Heat Rejection

The previous section presented the solution for the fin-tube radiating effectiveness of a three-tube system with the center tube punctured. It is now desired to use this information to determine the total heat rejection of a shared-fin radiator panel with multiple tube circuits subject to loss of working fluid in one circuit. In applying η_p for the calculation of the total panel heat rejection, it is assumed that no two adjacent tubes are punctured and that no end tube is inoperative.

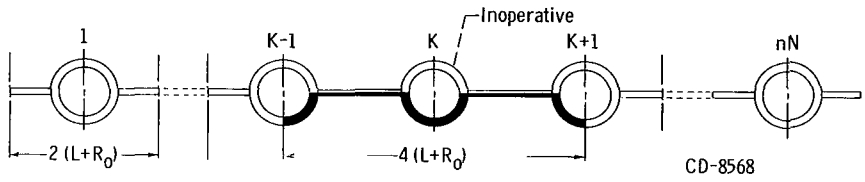

Figure 4. - Shared-fin-tube panel.

Figure 4 illustrates a radiator panel with tube number K inoperative. From previous considerations (eq. (24)), one side of the section of radiator formed by tubes numbered K-1, K, and K+1 (shaded in fig. 4), rejects an amount of heat equal to

$$Q_p = 2\eta_p Q_{id} \qquad (25)$$

If there are n tubes in each circuit, N circuits in the radiator panel, and one circuit is not operating, the remainder of the panel rejects the design amount of heat given by

$$Q_D = (nN - 2n)\eta_D Q_{id} \qquad (26)$$

where η_D is the design radiating effectiveness (e.g., ref. 4). Thus, the total panel heat rejection by a panel with N circuits, n tubes per circuit, and with one circuit inoperative is given by

$$Q_p^* = (nN - 2n)\eta_D Q_{id} + 2n\eta_p Q_{id} \tag{27}$$

Defining a total panel effectiveness η_p^* as

$$\eta_p^* = \frac{Q_p^*}{nNQ_{id}} \tag{28}$$

and substituting for Q_p^* from equation (27) result in the following expression for η_p^*:

$$\eta_p^* = \left(1 - \frac{2}{N}\right)\eta_D + \frac{2}{N}\eta_p \tag{29}$$

A quantity useful for the comparison of the heat-rejection characteristics of the shared-fin and simply segmented radiator systems is the ratio of punctured to design heat rejection. It is assumed for comparison purposes that the shared-fin and simply segmented concepts are applied to the same nonredundant radiator system operating at design conditions. For the shared fin, the ratio of punctured to design heat rejection is

$$\left(\frac{Q_p^*}{Q_D^*}\right)_{SF} = \frac{\eta_p^* nNQ_{id}}{\eta_D nNQ_{id}} = \frac{\eta_p^*}{\eta_D} \tag{30}$$

Substituting for η_p^* from equation (29) and simplifying result in

$$\left(\frac{Q_p^*}{Q_D^*}\right)_{SF} = 1 - \frac{2}{N}\left(1 - \frac{\eta_p}{\eta_D}\right) \tag{31}$$

For the simply segmented radiator with one circuit out of N inoperative, the heat-rejection ratio is simply

$$\left(\frac{Q_p^*}{Q_D^*}\right)_{SS} = \frac{(N - 1)\eta_D Q_{id}}{N\eta_D Q_{id}}$$

or

$$\left(\frac{Q_p^*}{Q_D^*}\right)_{SS} = 1 - \frac{1}{N} \tag{32}$$

RESULTS AND DISCUSSION

Central Fin-Tube Configuration

Temperature variations. - Each solution of the energy equation (8) in conjunction with the equilibrium temperature equation (15) provides a distribution of temperature along the fin between the hot tube and the punctured tube. Some typical temperature profiles for the central fin-tube geometry of figure 1(a) (p. 2) are shown plotted in figure 5(a) for several values of N_c and L/R_o. The temperature ratio at $X = 1$ is the temperature ratio at the punctured tube (constant over tube surface).

For a constant value of L/R_o, increasing N_c lowers the local temperature as expected, since larger values of N_c correspond to lower conducting potential. At large N_c, the effect of interchange between fin and tube and between the operating and punctured tubes on the local temperature is quite important since radiation is the dominant mode of heat transfer. In fact at $L/R_o = 2$, the punctured (dead) tube picks up enough radiant energy so that some heat is actually conducted back into the fin, which results in the positive slope at $X = 1.0$.

In general, for a constant N_c, the local temperature is expected to decrease as L/R_o increases, since at larger L/R_o there is less interchange between a point on the fin and the tubes. At $N_c = 0.5$, however, the local temperature near the punctured tube ($X > 0.7$) for $L/R_o = 8$ is higher than for $L/R_o = 2$. At this value of N_c, conduction is the dominant mode of heat transfer along the fin and the effect of incident radiation from the tubes is negligible. Thus, the dead tube in both cases receives the same amount of heat by conduction. The tube at $L/R_o = 2$, however, has more surface area than at $L/R_o = 8$ and is better able to reject heat by radiation. As a result, the equilibrium temperature of the punctured tube is lower for $L/R_o = 2$ than for $L/R_o = 8$, which lowers the local temperature along the fin.

The equilibrium temperature (eq. (15)) of the punctured tube (temperature at $X = 1.0$) is plotted in figure 5(b) as a function of L/R_o for selected values of N_c. The curves are cut off at $L/R_o = 0.5$, because at low values of L/R_o the assumption of circumferentially constant punctured tube temperature may not be valid. The punctured tube temperature decreases with increasing N_c and increasing L/R_o (except at low N_c) and asymptotically

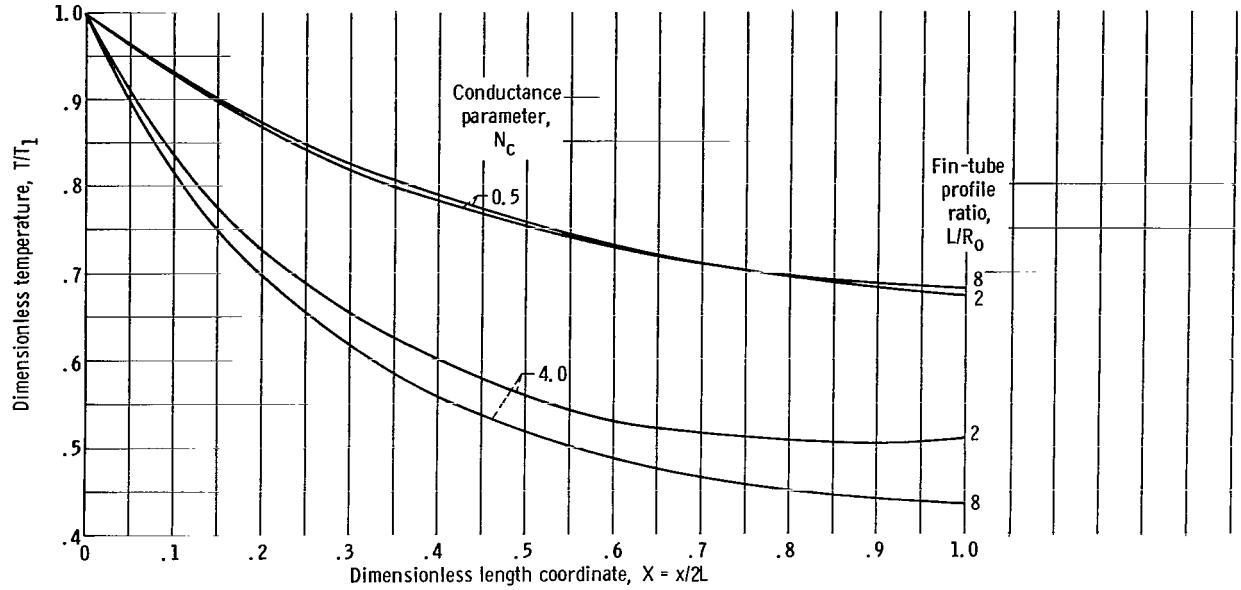

(a) Representative fin temperature profiles.

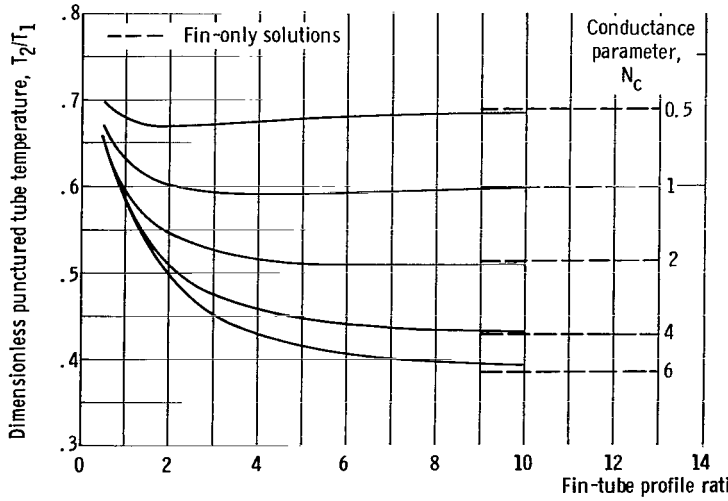

(b) Punctured-tube equilibrium temperature.

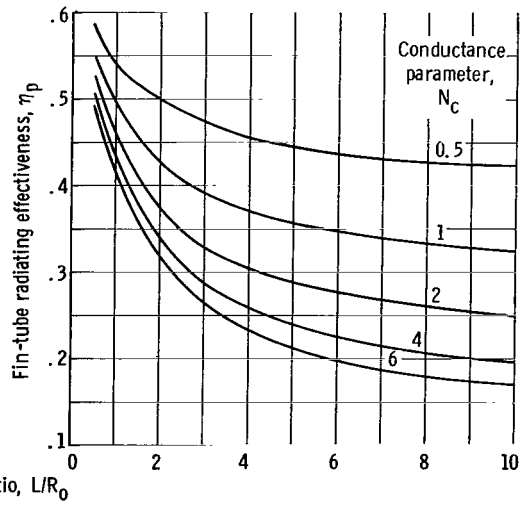

(c) Radiating effectiveness of punctured fin-tube segment.

Figure 5. - Results for central fin-tube configuration.

approach the terminal temperature of the fin-only solutions, that is, solutions for a fin of half width $2L + R_o$ with no interchange between tube and fin (ref. 8).

At the low values of N_c, the punctured tube temperature drops below the fin-only value and approaches it from below. The reason for this becomes clear when it is realized that the fin-only solution assumes that the heat-rejection surface area corresponding to the tube portion is $2R_o$ rather than πR_o. Hence, when conduction is the dominant mode of heat transfer (low N_c), the fin-only model is less able to reject the heat conducted into it than the fin-tube model. Consequently, the terminal temperature is higher

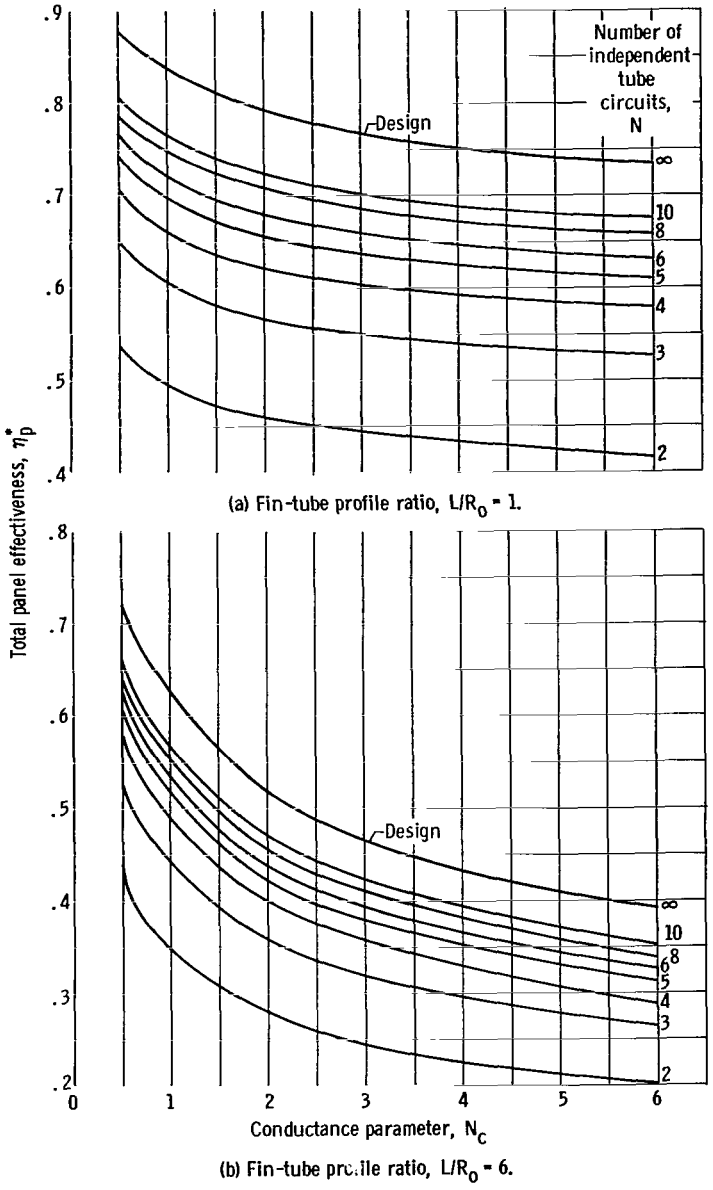

Figure 6. - Shared-fin radiator total panel effectiveness for central fin-tube configuration with one tube circuit punctured.

than the punctured tube temperature.

At the higher values of N_c, the effects of radiant interchange become dominant. Since the view factors from tube-to-tube and from fin-to-tube are higher for the fin-tube model, its temperature remains higher than the fin-only model for all L/R_o.

Fin-tube radiating effectiveness. - The radiating effectiveness of the punctured fin-tube segment (two tubes and associated shared fin) obtained from equation (24) is presented in figure 5(c). In general, the resulting trends are similar to those obtained for the design condition (ref. 4). For a given N_c, the thermal effectiveness decreases with increasing L/R_o. This variation is affected by the operating tubes in two ways. First, the hot tube rejects heat at the highest system temperature (T_1) and thus at the highest effectiveness. Hence, as the ratio of tube surface area to fin area decreases (increasing L/R_o), the fin-tube radiating effectiveness will decrease, since the influence of the hot tube is diminishing. Also, through radiant interchange, the hot tubes increase the local temperature along the fin. As L/R_o increases, the view factors between tube and fin decrease, which decreases the local fin temperature and lowers effectiveness. At a given L/R_o, increasing N_c also lowers the effectiveness since larger values of N_c correspond to lower fin temperatures as noted previously.

The total panel effectiveness is plotted as a function of conductance parameter and number of circuits for two values of L/R_o in figure 6. As expected, the increased redundancy of more tube circuits increases the total panel effectiveness. However, each additional circuit increases the total panel effectiveness by a diminishing amount as is

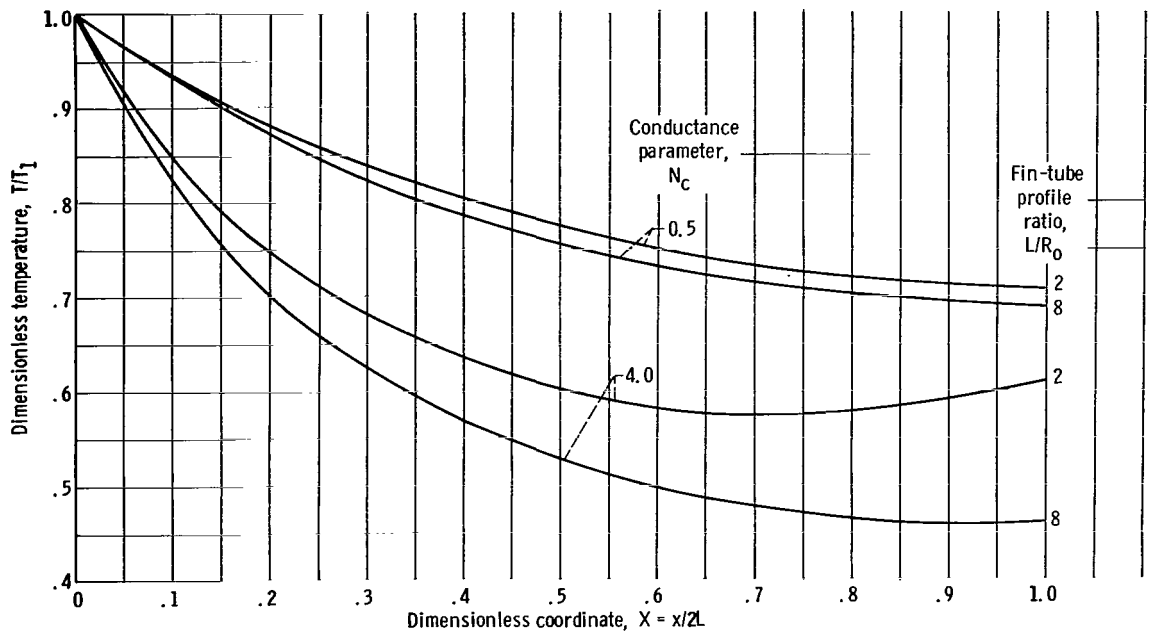

(a) Representative fin temperature profiles.

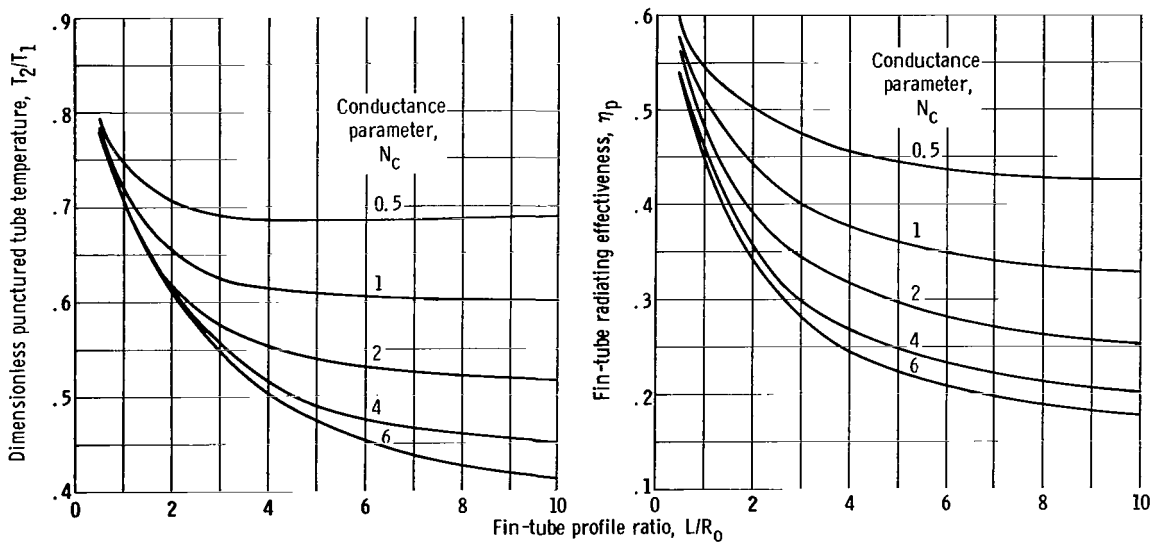

(b) Punctured-tube equilibrium temperature.

(c) Radiating effectiveness of punctured fin-tube segment.

Figure 7. - Results for open fin-tube configuration.

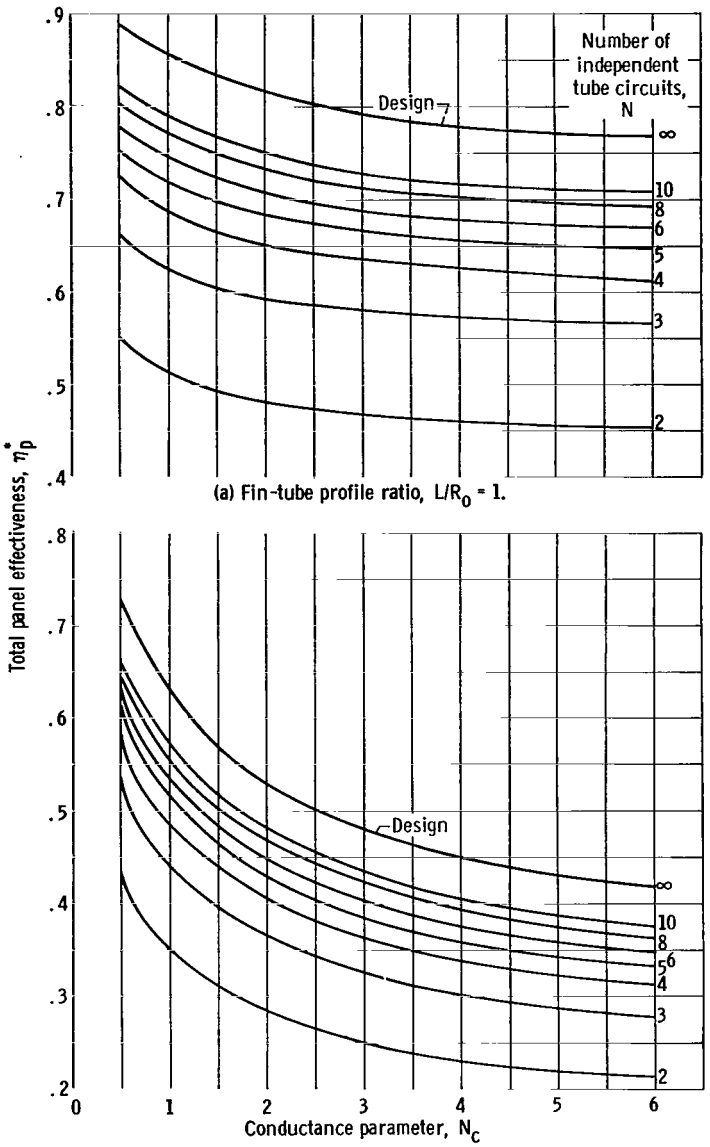

Figure 8. - Shared-fin radiator total panel effectiveness for open fin-tube configuration with one tube circuit punctured.

indicated by the convergence of the curves as N increases. This condition indicates that an optimum number of circuits might exist where the added weight and complexity involved in increasing N will offset any gains realized through the increased panel effectiveness.

The ratio of punctured to design total panel effectiveness for the central fin geometry can be obtained from the results of figure 6. For two circuits and an $L/R_o = 1$, the ratio varies from 0.56 to 0.62 over the range of N_c investigated. At the higher fin-tube profile ratio of $L/R_o = 6$, the ratio varied from 0.52 to 0.61. As the number of circuits increased to four, the ratio for both values of L/R_o varied from 0.74 to 0.81 over the range of conductance parameter investigated.

Open Fin-Tube Configuration

Results of typical temperature profiles, punctured-tube equilibrium temperature, fin-tube radiating effectiveness, and total panel effectiveness for the open fin-tube configuration (analyzed in appendix C) are presented in figures 7 and 8. Because of increased radiant interchange, the local temperatures along the fin are slightly higher than for the central fin. This results in slightly higher punctured-tube temperatures. Comparison of figures 7(c) and 8 with figures 5(c) and 6 indicates that very little difference exists between the open and the central fin for both the fin-tube radiating effectiveness (η_p) and total panel effectiveness (η_p^*). The ratio of punctured to design total panel effectiveness as a function of N, L/R_o, and N_c was essentially the same as for the central fin-tube geometry.

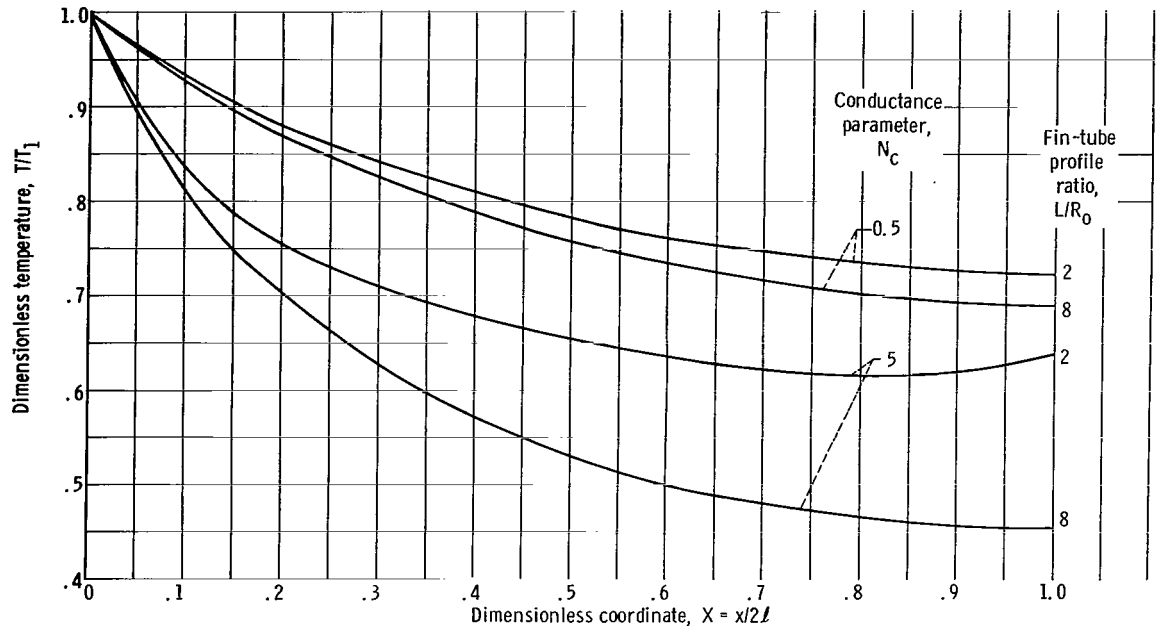

(a) Representative temperature profiles.

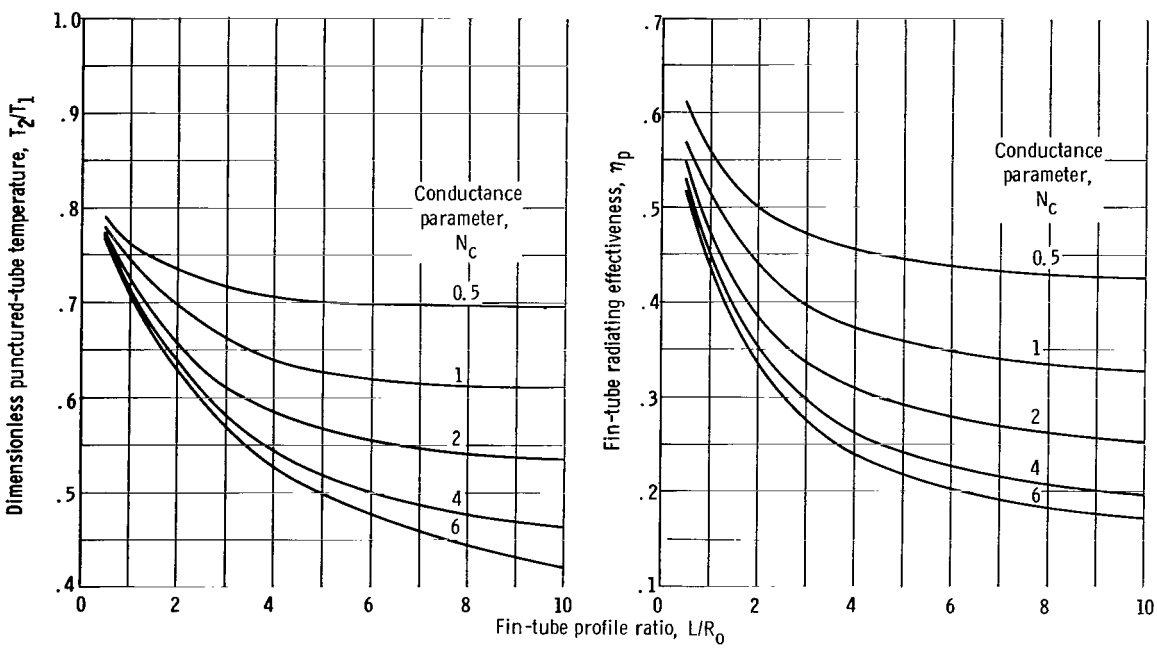

(b) Punctured tube equilibrium temperature. Ratio of tube side-wall to armor thickness, $\delta_s/\delta_a = 0.5$.

(c) Radiating effectiveness of punctured fin-tube segment. Ratio of tube side-wall to armor thickness, $\delta_s/\delta_a = 0.5$.

Figure 9. - Results for double fin-tube configuration.

Double Fin-Tube Configuration

Results of typical temperature profiles, punctured-tube equilibrium temperature, fin-tube radiating effectiveness, and total panel effectiveness for the double fin-tube configuration (appendix C) are presented in figures 9 and 10. The results are presented in terms of L/R_o rather than ℓ/R_o (see fig. 1(c), p. 2) since for equal tube diameters and tube wall thickness, equal L/R_o results in the same tube-centerline-to-fin-centerline distance for the three geometries. The increased amount of radiant interchange introduced by this geometry tends to maintain local fin temperatures at a slightly higher level than for the fin of the central fin tube. As a result, the equilibrium punctured-tube temperature is slightly higher for the double fin-tube geometry.

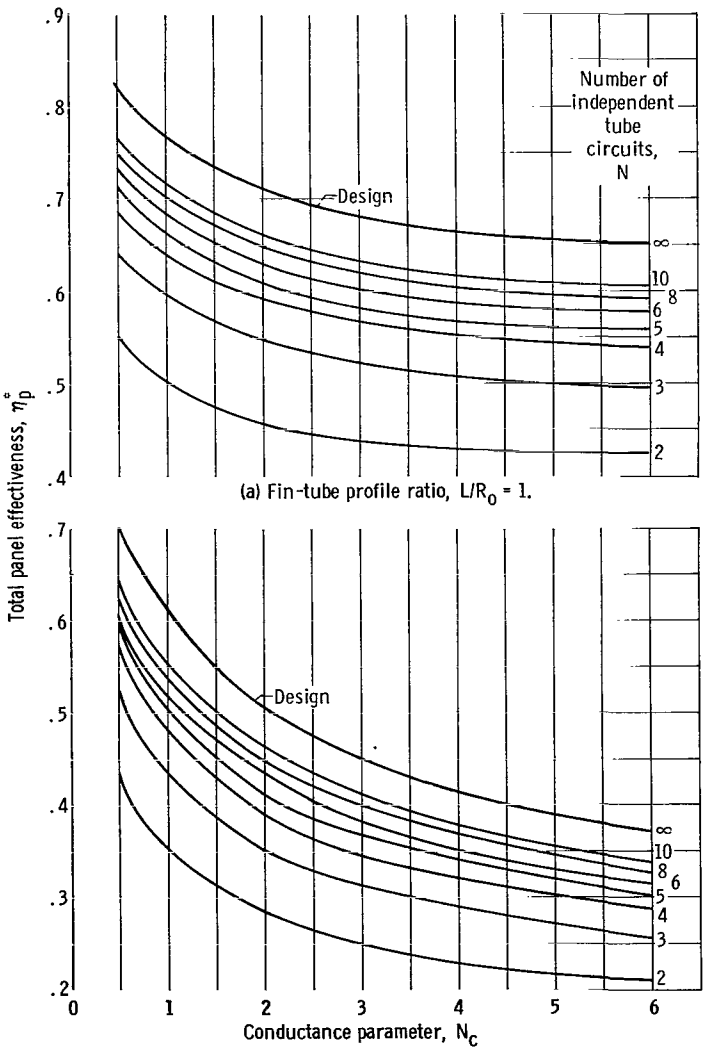

Figure 10. - Shared-fin radiator total panel effectiveness for double fin-tube configuration with one tube circuit punctured. Ratio of tube sidewall to armor thickness, δ_s/δ_a = 0.5.

Because of the ability of this configuration to act as a meteoroid bumper for both enclosed tube surfaces (appendix C), only a fraction of tube armor need be retained on the enclosed tube walls; that is, $\delta_s/\delta_a \leq 1$ (fig. 1(c)). A value of $\delta_s/\delta_a = 0.5$ was selected for the calculations in this report. Variation of δ_s/δ_a from 0.5 to 0 resulted, at most, in only a 3-percent difference in η_p. As a result of this reduced thickness of the tube sidewalls, at a given L/R_o, the ratio of tube surface area to fin surface area is lower for the double fin than for the central fin. This results in a slightly lower thermal effectiveness for the double fin at a given L/R_o and N_c (fig. 9(c)).

Figure 10 shows the total panel effectiveness of the double fin as a function of N_c and N for $L/R_o = 1$ and $L/R_o = 6$. As in the case of the central fin, the same general trend of increasing η_p^* with increasing N is evident. For two circuits and an

$L/R_o = 1$, the ratio of punctured panel effectiveness to design effectiveness ($N = \infty$) varies from 0.65 to 0.67 over the range of conductance parameter investigated. For the fin-tube profile ratio of $L/R_o = 6$, the ratio varied from 0.57 to 0.63. For four circuits, the ratio of effectiveness for both values of L/R_o varied from 0.78 to 0.83 over the range of N_c investigated.

Comparison of Results

A comparison of the heat-rejection results of the central, open, and double fin-tube geometries can be obtained by using the results of figures 6, 8, and 10 as expressed in terms of the ratio of punctured total panel effectiveness to design total panel effectiveness. For the lowest value of N, the ratio of effectiveness for the double fin geometry was slightly greater (7 to 9 percent) than for the central and open fin geometries over the range of values of N_c and L/R_o investigated. The differences decreased as the number of circuits increased. For two circuits, the ratio of effectiveness varied from 0.52 to 0.62 for the central and open fin-tube geometries and from 0.57 to 0.67 for the double fin-tube geometry. For four circuits, the central and open fin-tube geometries varied from 0.74 to 0.81 and the double fin-tube geometry varied from 0.78 to 0.83.

A comparison of the heat-rejection characteristics of the three shared-fin radiator configurations with those of the simply segmented approach (eqs. (31) and (32)) is shown in figure 11 for a range of the values of N_c and L/R_o. As expected, the additional circuits result in an increase in Q_p^*/Q_D^*. For all choices of N_c and L/R_o investigated, the double fin-tube geometry yielded the largest value of Q_p^*/Q_D^*, while the open fin-tube geometry yielded the least. The difference between the three geometries is at most only about 5 percent, however, which indicates no large advantage for any one of the geometries.

Comparison of the shared-fin with the simply segmented radiator indicates that the greatest advantage for the shared fin occurs for the minimum number of circuits ($N = 2$). At this condition, the shared fin Q_p^*/Q_D^* is from 10 to 30 percent greater than for the simply segmented case. As the number of circuits is increased, the difference between the shared-fin and simply segmented radiator diminishes. At $N = 4$, the shared fin's advantage has been reduced to 3 to 9 percent. It can also be observed (fig. 11) that the shared-fin radiator will require fewer circuits than a simply segmented one for the source value of Q_p^*/Q_D^*.

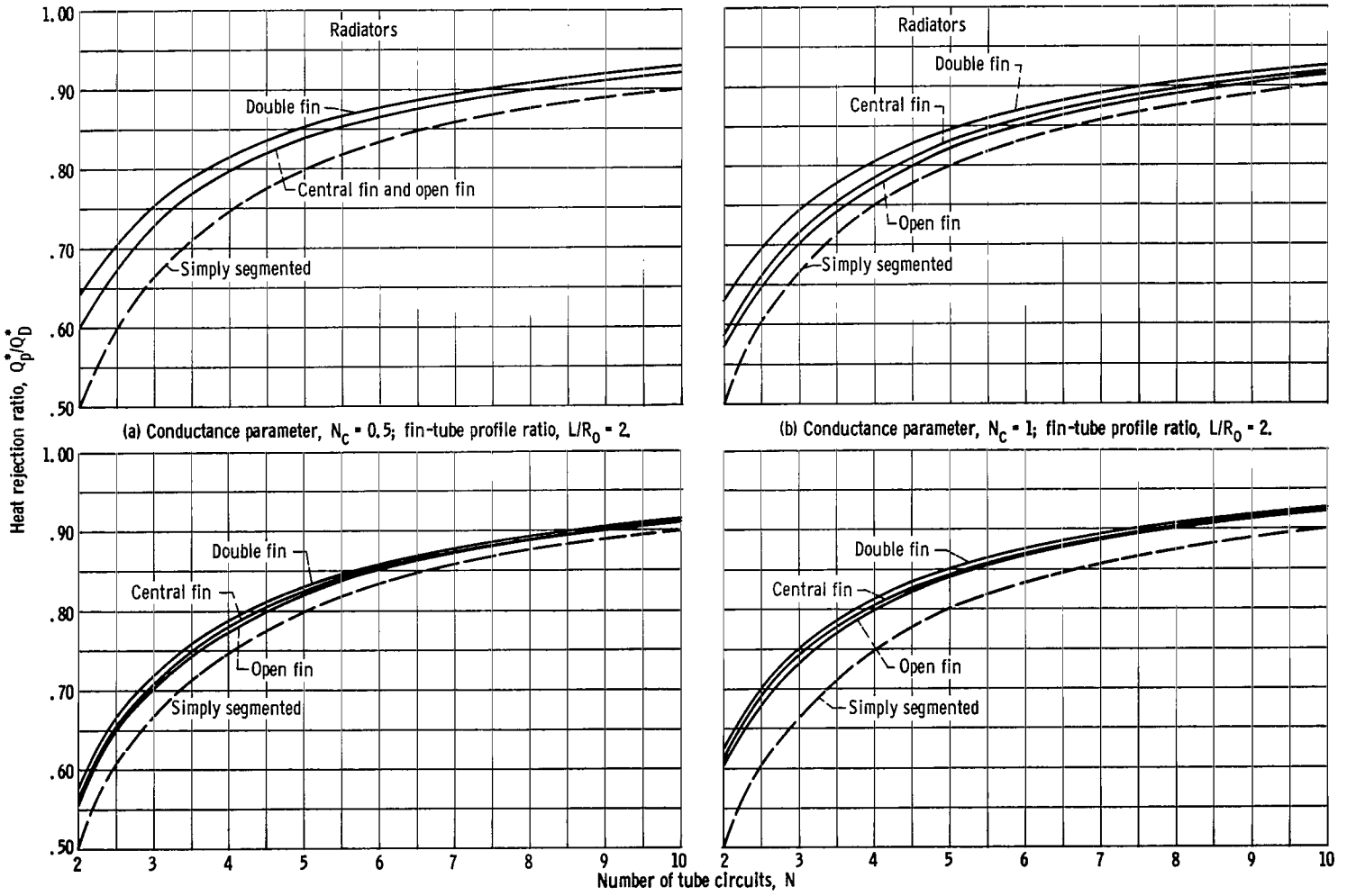

(a) Conductance parameter, $N_C = 0.5$; fin-tube profile ratio, $L/R_0 = 2$.

(b) Conductance parameter, $N_C = 1$; fin-tube profile ratio, $L/R_0 = 2$.

(c) Conductance parameter, $N_C = 1$; fin-tube profile ratio, $L/R_0 = 6$.

(d) Conductance parameter, $N_C = 0.5$; fin-tube profile ratio, $L/R_0 = 6$.

Figure 11. - Ratio of punctured to design total panel effectiveness with one tube circuit punctured.

SUMMARY OF RESULTS

The foregoing analyses have provided results of heat-transfer characteristics for three radiator finned-tube configurations used in a shared-fin radiator panel. Comparisons on the basis of a two circuit system with one circuit inoperative showed that, for fin profile ratios and conductance parameter values of practical interest, the heat-transfer performance of the three geometries were generally comparable. The ratio of heat rejection after puncture to design heat rejection for two circuits ranged from around 0.55 to 0.65 for the central, open, and double fin-tube geometries considered.

Comparison of the shared-fin results with those for the simply segmented radiator for the case of one circuit punctured showed that, over the range of conditions investigated, the shared-fin arrangement offers an advantage that decreases as the number of circuits increases. For two independent circuits, the shared-fin heat rejection after puncture of one circuit is from 10 to 30 percent greater than for the simply segmented radiator. For four circuits, the advantage of the shared fin is reduced to 3 to 9 percent.

Lewis Research Center,
National Aeronautics and Space Administration,
Cleveland, Ohio, June 8, 1966,
120-27-04-36-22.

APPENDIX A

SYMBOLS

A	surface area, sq ft
F	view factor for radiation heat exchange
k	thermal conductivity, Btu/(hr)(ft)(^{o}R)
L	minimum fin half width, ft
L/R_o	fin-tube profile ratio
ℓ	actual fin half width, $\ell = L + \delta_a(1 - \delta_s/\delta_a)$, ft
N	number of independent tube circuits (original design)
N_c	conductance parameter, $\sigma\ell^2T_1^3/kt$
n	number of tubes per circuit
Q	heat flow, Btu/hr
R_b	base surface half width, ft
R_o	tube outer radius, ft
T	temperature, ^{o}R
t	fin half thickness (full thickness for double fin), ft
X	dimensionless length coordinate, x/2L or x/2ℓ
x	length coordinate, ft
Y	dimensionless length coordinate, y/2ℓ
y	length coordinate, ft
Z	fin and tube axial length, ft
δ_a	tube armor thickness, ft
δ_s	tube side-wall thickness, ft
η	radiating effectiveness
θ	dimensionless temperature, T/T_1
σ	Stefan-Boltzman constant, 0.173×10^{-8} Btu/(hr)(sq ft)(^{o}R^4)

Subscripts:

cond	conduction
D	design condition
E	emitted
f	fin
i	incident
id	ideal
p	punctured condition
R	rejection
SF	shared fin
SS	simply segmented
w	inner tube wall
x, X	position on fin (lower fin for double fin geometry)
y, Y	position on upper fin for double fin geometry
1, 2, 3	base surfaces, see fig. 1(a)

Superscript:

*	total panel

APPENDIX B

VIEW FACTORS

The general method of determining view factors between differential cylindrical elements of infinite length is presented in reference 9. This method is directly applicable to the geometries investigated in the previous analysis under the assumption of infinite axial dimensions. This section summarizes the various view factors needed for the complete specification in terms of the dimensionless coordinate X, the fin temperature profiles, the punctured tube temperature, and the fin-tube effectiveness equations.

Central Fin-Tube Geometry (Fig. 1(a))

Differential element on the fin to tube 1:

$$F_{X-1} = \frac{1}{2}\left\{1 - \frac{\left[\left(2X + \frac{R_o}{L}\right)^2 - \left(\frac{R_o}{L}\right)^2\right]^{1/2}}{2X + \frac{R_o}{L}}\right\} \tag{B1}$$

Differential element on the fin to tube 2:

$$F_{X-2} = \frac{1}{2}\left\{1 - \frac{\left[\left(2 - 2X + \frac{R_o}{L}\right)^2 - \left(\frac{R_o}{L}\right)^2\right]^{1/2}}{2 - 2X + \frac{R_o}{L}}\right\} \tag{B2}$$

Tube to tube:

$$F_{1-2} = F_{2-1} = 1 - \frac{2}{\pi}\left(1 + \frac{4}{\frac{R_o}{L}} \int_0^1 F_{X-1}\, dX\right) \tag{B3}$$

Open Fin-Tube Geometry (Fig. 1(b))

Differential element on the fin to tube 1:

$$F_{X-1} = \frac{1}{\left(1 + 2\frac{L}{R_o}X\right)^2 + 1} \tag{B4}$$

Differential element on the fin to tube 2:

$$F_{X-2} = \frac{1}{\left[1 + 2(1 - X)\frac{L}{R_o}\right]^2 + 1} \tag{B5}$$

Tube to tube:

$$F_{1-2} = F_{2-1} = 1 - \frac{1}{\frac{\pi}{2} + 1}\left(4\frac{L}{R_o}\int_0^1 F_{X-1}\,dX + 1\right) \tag{B6}$$

Double Fin-Tube Geometry (Fig. 1(c))

Differential element on lower fin to tube 1:

$$F_{X-1} = \frac{1}{2}\left\{1 - \frac{X}{\left[X^2 + \left(\frac{R_o}{\ell}\right)^2\right]^{1/2}}\right\} \tag{B7}$$

Differential element on lower fin to tube 2:

$$F_{X-2} = \frac{1}{2}\left\{1 - \frac{1 - X}{\left[(1 - X)^2 + \left(\frac{R_o}{\ell}\right)^2\right]^{1/2}}\right\} \tag{B8}$$

Differential element on lower fin to differential element on upper fin:

$$F_{X-Y} = \frac{1}{2}\left\{\frac{\left(\frac{R_o}{\ell}\right)^2}{\left[(Y - X)^2 + \left(\frac{R_o}{\ell}\right)^2\right]^{3/2}}\right\} dY \tag{B9}$$

Tube block to tube block:

$$F_{1-2} = F_{2-1} = \left[1 + \left(\frac{\ell}{R_o}\right)^2\right]^{1/2} - \frac{\ell}{R_o} \tag{B10}$$

APPENDIX C

HEAT-TRANSFER ANALYSIS FOR OPEN AND DOUBLE FIN-TUBE GEOMETRIES

Open Fin-Tube Geometry

The model chosen for the derivation of the equations describing the heat-rejection characteristics for the open fin-tube geometry is shown in figure 1(b) (p. 2). As was the case with the central fin, the system is symmetrical about the centerline of tube 2. Since interchange between fin and tubes is restricted to one surface of the fin, however, the system is not symmetrical about the fin centerline. Consequently, the elemental volume about which the heat balance is taken is of thickness 2t. A heat balance about 2tZ dx yields

$$Q_{cond} + Q_i = Q_{cond} + \frac{dQ_{cond}}{dx} dx + Q_E \tag{C1}$$

The terms in equation (C1) can be expressed as follows:

$$Q_i = \sigma F_{x-1} T_1^4 Z \, dx + \sigma F_{x-2} T_2^4 Z \, dx$$

$$Q_{cond} = -k \, 2tZ \frac{dT}{dx}$$

and

$$Q_E = 2\sigma T^4 Z \, dx$$

Substituting these into equation (C1) and nondimensionalizing as before yield

$$\frac{d^2\theta}{dX^2} = 2N_c\left(2\theta^4 - F_{X-1} - F_{X-2}\theta_2^4\right) \tag{C2}$$

A heat balance about the punctured tube yields the following expression for θ_2:

$$\theta_2^4 = F_{1-2} + \frac{2\,\frac{L}{R_o}}{\left(\frac{\pi}{2}+2\right)} \int_0^1 F_{X-2}\theta^4\, dX - \frac{\frac{L}{R_o}}{N_c\left(\frac{\pi}{2}+2\right)} \frac{d\theta}{dX}\Bigg|_{X=1} \tag{C3}$$

Simultaneous solution of equations (C2) and (C3), subject to the boundary conditions $\theta(0) = 1$ and $\theta(1) = \theta_2$, yields the temperature distribution and punctured tube temperature for the open fin-tube configuration.

From the definition of fin-tube radiating effectiveness given in the ANALYSIS section and the temperature distribution derived previously, the following expression can be derived for the effectiveness of the open fin-tube geometry:

$$\eta_p = \frac{\frac{\pi}{2}+1}{4\left(\frac{L}{R_o}+1\right)}\left(1 - F_{1-2}\theta_2^4\right) + \frac{1}{4\left(\frac{L}{R_o}+1\right)} - \frac{\frac{L}{R_o}}{2\left(\frac{L}{R_o}+1\right)} \int_0^1 F_{X-1}\theta^4\, dX - \frac{\frac{L}{R_o}}{4N_c\left(\frac{L}{R_o}+1\right)} \left(\frac{d\theta}{dX}\right)_{X=0} \tag{C4}$$

Double Fin-Tube Geometry

The double fin-tube geometry shown in figure 1(c) (p. 2) has the ability to act as a bumper screen that will afford protection against meteoroids on both faces of the radiator tube. The analysis for the fin temperature distribution of this configuration is more complex than the previously analyzed configurations because of the presence of two nonisothermal surfaces. The inclusion of the interchange between these two surfaces results in an integro-differential equation.

A heat balance about $tZ\,dx$ yields, as before,

$$Q_{cond} + Q_i = Q_{cond} + \frac{dQ_{cond}}{dx}\,dx + Q_E \tag{C5}$$

The terms in equation (C5) can be expressed as follows:

$$Q_{cond} = -k\,tZ\,\frac{dT}{dx}$$

$$Q_i = \sigma Z\, dx \int_0^{2\ell} F_{x-y} T_y^4\, dy + \sigma F_{x-1} T_1^4 Z\, dx + F_{x-2} T_2^4 Z\, dx$$

and

$$Q_E = 2\sigma T^4 Z\, dx$$

Substituting these values into equation (C5) and introducing the same nondimensional quantities as before yield

$$\frac{d^2\theta}{dX^2} = 2N_c \left(4\theta^4 - 2 \int_0^1 F_{X-Y} \theta^4\, dY - F_{X-1} - F_{X-2} \theta_2^4 \right) \tag{C6}$$

A heat balance about the punctured tube gives

$$\theta_2^4 = \frac{F_{1-2}}{1 + \dfrac{R_b}{R_o}} + \frac{2}{\dfrac{R_o}{\ell} + \dfrac{R_b}{\ell}} \int_0^1 F_{X-2} \theta^4\, dX - \frac{1}{2N_c} \left(\frac{\ell}{R_o + R_b} \right) \left(\frac{d\theta}{dX} \right)_{X=1} \tag{C7}$$

where

$$\ell = L + \left(1 - \frac{\delta_s}{\delta_a} \right) \delta_a$$

and

$$R_o \,/\, R_b + \left(1 - \frac{\delta_s}{\delta_a} \right) \delta_a$$

The parameter δ_s/δ_a is introduced to define the fraction of armor thickness retained on the enclosed side of the tube (fig. 1(c)) (p. 2). A value of $\delta_s/\delta_a = 0.5$ was selected for this investigation as being a typical value obtained for radiators associated with high electrical output powerplants (ref. 10). For this value of δ_s/δ_a, a value for δ_a of 0.353 inch was determined by using existing meteoroid protection criterion. An inner diameter was chosen to be 0.75 inch.

The definition of fin-tube radiating effectiveness for the double fin tube is the same as the two other geometries. Application of this definition results in

$$\eta_p = \frac{1}{2}\left(\frac{1}{1+\frac{\ell}{R_o}}\right)+\left(\frac{\frac{\ell}{R_o}}{1+\frac{\ell}{R_b}}\right)\int_0^1 \theta^4\, dX + \frac{1}{2}\left(\frac{1}{1+\frac{\ell}{R_b}}\right)\theta_2^4 \qquad \text{(C8)}$$

REFERENCES

1. Sparrow, E. M.; and Eckert, E. R. G.: Radiant Interaction Between Fin and Base Surfaces. J. Heat Transfer, vol. 84, no. 1, Feb. 1962, pp. 12-18.

2. Sparrow, E. M.; and Minkowycz, W. J.: Heat-Transfer Characteristics of Several Radiator Finned-Tube Configurations. NASA TN D-1435, 1962.

3. Haller, Henry C.; Wesling, Gordon C.; and Lieblein, Seymour: Heat-Rejection and Weight Characteristics of Fin-Tube Space Radiators with Tapered Fins. NASA TN D-2168, 1964.

4. Haller, Henry C.: Comparison of Heat-Rejection and Weight Characteristics of Several Radiator Fin-Tube Configurations. NASA TN D-2385, 1964.

5. Diamond, P. M.; and Hopson, G. D.: Heat Rejection in Space. Pt. 5 of Short Course in Space Power Plants, University of California, July 1961.

6. Lieblein, Seymour: Special Requirements on Power Generation Systems for Electric Propulsion. Proceedings of the NASA-University Conference on the Science and Technology of Space Exploration. NASA SP-11, vol. 2, 1962, pp. 157-166.

7. English, Robert E.; and Guentert, Donald C.: Segmenting of Radiators for Meteoroid Protection. ARS J., vol. 31, no. 8, Aug. 1961, pp. 1162-1164.

8. Lieblein, Seymour: Analysis of Temperature Distribution and Radiant Heat Transfer Along a Rectangular Fin of Constant Thickness. NASA TN D-196, 1959.

9. Sotos, Carol J.; and Stockman, Norbert O.: Radiant-Interchange View Factors and Limits of Visibility for Differential Cylindrical Surfaces with Parallel Generating Lines. NASA TN D-2556, 1964.

10. Haller, Henry C.: Analysis of a Double Fin-Tube Flat Condenser-Radiator and Comparison with a Central Fin-Tube Radiator. NASA TN D-2558, 1964.

"The aeronautical and space activities of the United States shall be conducted so as to contribute . . . to the expansion of human knowledge of phenomena in the atmosphere and space. The Administration shall provide for the widest practicable and appropriate dissemination of information concerning its activities and the results thereof."

—NATIONAL AERONAUTICS AND SPACE ACT OF 1958

NASA SCIENTIFIC AND TECHNICAL PUBLICATIONS

TECHNICAL REPORTS: Scientific and technical information considered important, complete, and a lasting contribution to existing knowledge.

TECHNICAL NOTES: Information less broad in scope but nevertheless of importance as a contribution to existing knowledge.

TECHNICAL MEMORANDUMS: Information receiving limited distribution because of preliminary data, security classification, or other reasons.

CONTRACTOR REPORTS: Technical information generated in connection with a NASA contract or grant and released under NASA auspices.

TECHNICAL TRANSLATIONS: Information published in a foreign language considered to merit NASA distribution in English.

TECHNICAL REPRINTS: Information derived from NASA activities and initially published in the form of journal articles.

SPECIAL PUBLICATIONS: Information derived from or of value to NASA activities but not necessarily reporting the results of individual NASA-programmed scientific efforts. Publications include conference proceedings, monographs, data compilations, handbooks, sourcebooks, and special bibliographies.

Details on the availability of these publications may be obtained from:

SCIENTIFIC AND TECHNICAL INFORMATION DIVISION

NATIONAL AERONAUTICS AND SPACE ADMINISTRATION

Washington, D.C. 20546